Phase behavior of a reversibly assembling system in two dimensions: A Monte Carlo simulation study

Wen-Ze Ouyang and Reinhard Hentschke*,†
Fachbereich Mathematik und Naturwissenschaften, Bergische Universität, D-42097 Wuppertal, Germany
(Received 27 October 2008; published 13 March 2009)

Using Monte Carlo simulation, we investigate the structural phase behavior of a continuum molecular model for self-assembling semiflexible equilibrium polymers in two dimensions. Particle-particle interaction is modeled via a Lennard-Jones potential with tunable anisotropic attraction. Depending on the strength of the anisotropy, we find the formation of reversible networks as well as stiff rodlike aggregates. The phase transition observed in the presence of the network structures is compared to predictions of the Tlusty-Safran defect model.

DOI: 10.1103/PhysRevE.79.031503 PACS number(s): 64.70.F−, 82.35.−x, 05.50.+q, 61.20.Qg

I. INTRODUCTION

Additional anisotropic interparticle interaction in models of otherwise simple fluids may lead to rather complex phase behavior. Anisotropic attractive interaction usually causes the formation of reversible chains, rings, branched structures, or networks as in dipolar fluids [1–3]. These aggregates add complexity to an extent that thus far has prevented the theoretical computation or even simulation of complete phase diagrams.

In the present work, we study, via Monte Carlo (MC) computer simulation, a model with anisotropic and variable dispersion attraction between otherwise r^{-12}-repulsive particles in two dimensions. Structure, dielectric or magnetic properties, and phase behavior of similar two-dimensional (2D) dipolar fluids have been investigated via computer simulation in the past, initially because of the reduced computational effort compared to three dimensions (3D) (e.g., [4,5]) and later because of the increased interest in dimensional effects as well as in applications involving monolayers or thin films (e.g., [6–10]).

Originally the 3D version of the present model was introduced as a computationally inexpensive but effective model representing stacking amphipilic molecules in solution [11]. Akin to the monomers in the model, real stacking amphiphilic molecules may form linear aggregates, bend-elastic polydisperse rods, which due to excluded volume interaction exhibit liquid crystalline phases. In particular, it was shown that the model potential is a good description for the isotropic-nematic-hexagonal columnar phase behavior of a real stacking amphiphile, a triphenylene derivative, whose phase behavior was studied in great detail by Boden and co-workers [12]. It was then realized that this potential, with its tunable anisotropic attraction, may be suitable to study the connection between essentially lyotropic liquid crystalline phase behavior in reversibly assembling systems and ordering behavior typically observed in dipolar liquids or even in simple liquids described via Lennard-Jones interactions. In a subsequent publication, we studied the transition from the above lyotropic liquid crystalline phase behavior, occurring for strong anisotropy, to ordinary gas-liquid (GL) phase behavior, occurring when the interaction anisotropy is weak [13]. The 2D version of the model is interesting because it exhibits, in a certain range of the parameter controlling interaction anisotropy, the formation of reversible networks in conjunction with dilute-dense phase separation. Here we map out a large portion of this system's phase behavior. In particular, we discuss the above dilute-dense phase separation in the presence of reversible network structures in relation to a defect model suggested by Tlusty and Safran [14] as well as in terms of GL phase separation of equilibrium polymers.

II. MODEL AND SIMULATION METHODOLOGY

The classical fluid model studied in the following consists of particles interacting via a modified Lennard-Jones (LJ) potential (here and in the following we use LJ units):

$$u_{ij} = 4[r_{ij}^{-12} - \mu|f|^{\nu} r_{ij}^{-6}], \tag{1}$$

where

$$f = \frac{(\vec{n}_i \cdot \vec{r}_{ij})(\vec{n}_j \cdot \vec{r}_{ij})}{r_{ij}^2} \tag{2}$$

($\mu, \nu > 0$), and $\vec{n}_i$ is a unit vector assigning an orientation to each monomer i, i.e., the attractive part of the potential is anisotropic. Previously we have used this potential to describe a 3D model fluid [11,13]. Now the position vectors $\vec{r}_{ij}$ are confined to a 2D plane. No such restriction applies to the orientation vectors $\vec{n}_i$, however. The anisotropy factor, $|f|$, is unity if both $\vec{n}_i$ and $\vec{n}_j$ are parallel or antiparallel to $\vec{r}_{ij}$, the vector connecting the monomers i and j. If either $\vec{n}_i$ or $\vec{n}_j$ or both are perpendicular to $\vec{r}_{ij}$, then $|f|=0$. Notice that the magnitude of ν controls the angular width of the attraction, whereas μ controls the strength of the attraction.

We note that simulations using the potential in Eqs. (1) and (2) with different values for μ may be mapped onto the case $\mu=1$ using the scaled quantities defined via

$$T^{\mathrm{scal}} = \mu^{-2} T \tag{3}$$

and $\vec{r}^{\,\mathrm{scal}} = \mu^{1/6}\vec{r}$ or

*Author to whom correspondence should be addressed.
†hentschk@uni-wuppertal.de; URL: http://constanze.materials.uni-wuppertal.de

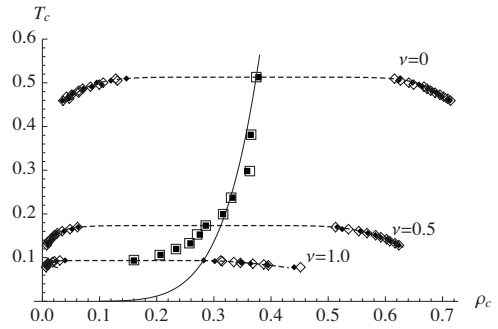

FIG. 1. Phase behavior in the T-ρ plane for different ν starting from $\nu=0.0$ (top) to $\nu=1.0$ (bottom) in steps of 0.1. Closed (open) diamonds represent coexisting densities obtained upon compression (expansion). Dashed lines are the scaling-law approximations used to determine the GL critical points (squares). The solid line is the scaling relation explained in the text.

$$\rho^{\text{scal}} = \mu^{-d/6}\rho, \tag{4}$$

where T and ρ are the temperature and particle number density, respectively. This is because the NVT configuration probability density is invariant under this transformation. Here $d=2$, whereas $d=3$ for the 3D system studied in Ref. [13]. In order to avoid complicated notation, we use T instead of T^{scal} and ρ instead of ρ^{scal} from here on (i.e., $\mu=1$).

As before (cf. [13]), the configurational averages presented in this work are obtained via ordinary METROPOLIS MC. For a randomly selected monomer, translation or rotation is attempted with equal probability. The maximum translation and rotation of the monomer are chosen so that about half the trial moves are accepted by the METROPOLIS criterion, $\min(1,\exp[-\Delta U/T]) \geqslant \xi$, where $\xi \in (0,1)$ is a random number, and $\Delta U = U_{\text{new}} - U_{\text{old}}$ is the potential energy difference between the new and the old configuration. Notice that the number of monomers, N, the monomer number density, $\rho=N/V$, and the temperature, T, are constants. Monomer-monomer interactions are cut off at $r_{\text{cut}}=5.7$ using the minimum image convention. Notice that due to the anisotropic r^{-6} interaction (for $\nu \neq 0$), we do not employ the usual long-range corrections. The number of monomers, N, is 256. Initially we place the randomly oriented monomers on a simple cubic lattice in a 2D cubic simulation box. The system is heated into a fluid phase of nonassociated monomers and subsequently cooled to the desired temperature.

III. RESULTS

Figure 1 shows the GL phase behavior in the T-ρ plane for different values of ν. Here $\nu=0$ corresponds to the GL coexistence curve in the pure LJ system in 2D with truncated interaction. GL phase coexistence curves are obtained via the following procedure. We carry out a large number of NVT simulations along an isotherm, which allows us to employ the Maxwell construction to obtain the coexisting densities for the pure gas and the pure liquid, respectively. Specifically, we do fit the isotherm data for which the compressibility is positive using a modification of van der Waal's equation of state, i.e., $P=NT/(V-Na_1)+a_0/(V-Na_2)-a_0/(V-Na_3)$, where the a_i $(i=0,1,2,3)$ are adjustable parameters [15]. The coexisting densities are obtained via this equation. Repeating this procedure for a series of temperatures yields the GL coexistence curve, which we analyze using the well known scaling relations, i.e., $\rho_L-\rho_G \approx A_o|t|^{\beta}$ and $(\rho_L+\rho_G)/2 \approx \rho_c + D_o|t|^{1-\alpha}$ $(t=T/T_c-1)$ [16], in conjunction with the Ising values of the critical exponents $\alpha=0$ and $\beta=0.125$, to extract the critical point parameters. Notice that the closed and the open symbols in Fig. 1 correspond to compression and subsequent expansion along an isotherm, respectively.

We note that in Ref. [17] the authors study the GL transition of the 2D LJ fluid with truncated interactions using MC simulations in conjunction with finite-size scaling techniques. They obtain $T_c=0.50\pm0.02$, which is in good agreement with the $\nu=0$ curve in Fig. 1 where $T_c \approx 0.51$. The excellent agreement is, however, somewhat exaggerated, because the cutoff in Ref. [17] is smaller, which tends to lower T_c due to the neglect of attractive interaction. In addition, using the Ising exponents in the above scaling relations may not be quite appropriate close to criticality due to the finite-size truncation of critical fluctuations. Nevertheless, comparison with corresponding results for T_c obtained via the mean-field exponents and including correction terms indicates that the size of the symbols in Fig. 1 is a reasonable estimate for the error due to the uncertainties in the fit procedure applied to the coexisting densities.

When ν is increased we observe a shift of the critical point to lower temperatures and densities analogous to the previous behavior in 3D (cf. Fig. 1 in Ref. [13]). As before, this may be understood partially by replacing $|f|^{\nu}$ in the interaction potential by its rotational in-plane average in the weak interaction limit given by $\lambda = \pi^{-2}\int d\theta_i d\theta_j |f|^{\nu} = \pi^{-2}(\int d\phi \cos^{\nu}\phi)^2 = \pi^{-2}\{\Gamma[(1+\nu)/2]/\Gamma[1+\nu/2]\}^2$. Here $\Gamma(x)$ is the Gamma function. Just as in the case of μ, we may now map systems with different ν onto a LJ reference system, i.e., $\nu=0$, via

$$T_{\text{LJ}} = \lambda^{-2}T \quad \text{and} \quad \rho_{\text{LJ}} = \lambda^{-1/3}\rho. \tag{5}$$

The mapping applies as long as the anisotropy factor does not alter the local structure significantly compared to the LJ system. Combining these two equations yields $T=(T_{\text{LJ}}/\rho_{\text{LJ}}{}^6)\rho^6$. This is the solid line in Fig. 1. The solid lines in the two panels of Fig. 2 are the direct comparison of this scaling, i.e., Eq. (5), to the simulation results for the critical quantities. We note that the agreement between the scaling and the simulation is quite reasonable for small ν. (In the case of the critical temperature the agreement is good for all ν shown in the graph.) The deviations for larger ν, which are very similar in the 3D system (cf. Figs. 1 and 2 in Ref. [13]), were explained previously as being due to the formation of reversible chains (cf. below).

We employ various functions to characterize the structural properties of our model. The quantity

$$q_{\perp}^{\text{orient}} = \frac{1}{N}\left\langle \sum_{i=1}^{N} \frac{1}{2}(3\cos^2\theta_i - 1) \right\rangle, \tag{6}$$

where θ_i is the angle between $\vec{n}_i$ and the axis normal to the plane to which the particles are confined, is a measure of the

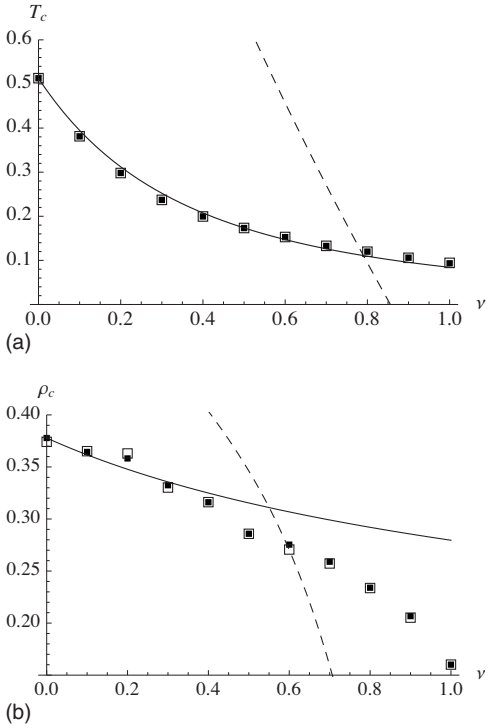

FIG. 2. Top: GL critical temperature, T_c, vs ν; bottom: GL critical density, ρ_c, vs ν. Closed and open symbols have the same meaning as in the previous figure. The solid lines are the power-law predictions of Eq. (5). The dashed lines are computed on the basis of Eqs. (11) and (12).

average out-of-plane tilt of the $\vec{n}_i$. Note that $q_\perp^{\text{orient}}=0$ if the particles are noninteracting and $q_\perp^{\text{orient}}=-1/2$ if all $\vec{n}_i$ are parallel to the plane. An example is shown in Fig. 3 showing $q_\perp^{\text{orient}}$ for $\nu=0.5$ and 2.0 versus ρ close to the respective critical temperature, i.e., $T=0.165$ and 0.092. At low densities $q_\perp^{\text{orient}}\approx 0$, as expected, because there is little interaction between particles and the $\vec{n}_i$ are isotropically oriented. As the density increases, the growing interaction forces the $\vec{n}_i$ into the plane. This general behavior is observed for all ν considered here.

Another useful order parameter is

$$q_\parallel^{\text{orient}} = \frac{2}{N(N-1)}\left\langle \sum_{i<j} (2\cos^2 \Delta\phi_{ij} - 1)\right\rangle, \tag{7}$$

where $\Delta\phi_{ij}$ is the perpendicular projection of the angle between $\vec{n}_i$ and $\vec{n}_j$ onto the plane. $q_\parallel^{\text{orient}}$ is a measure for nematic orientation of the $\vec{n}_i$ parallel to the plane. Figure 4 shows $q_\parallel^{\text{orient}}$ plotted versus ν at $T=0.092$ and $\rho=0.537$. Below $\nu \approx 1$ we find isotropic orientation of the $\vec{n}_i$ parallel to the plane. Two of the insets are simulation snapshots for $\nu=1.0$ and 1.1 showing isotropic equilibrium network structures, which we did not observe in the 3D case most likely due to the associated entropy loss [13]. (In 3D we merely find network structures apparently far from equilibrium.) Above $\nu=1.1$ a sudden change occurs. Rather stiff chains appear, suppressing junction formation and favoring alignment due to excluded volume interaction between them.

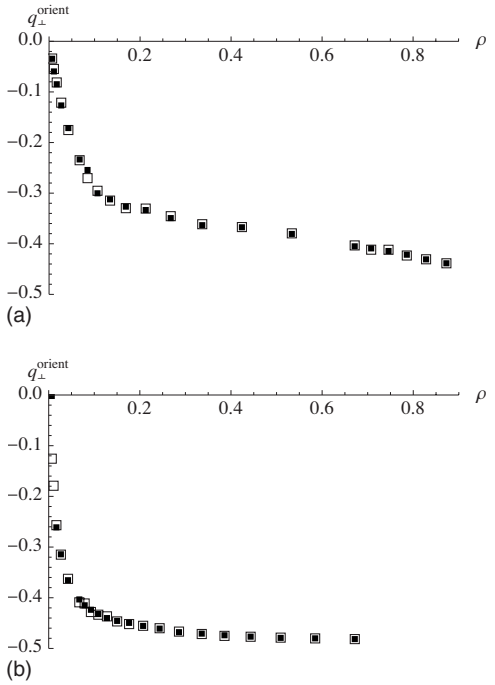

FIG. 3. Out-of-plane tilt $q_\perp^{\text{orient}}$ for $\nu=0.5$ (top) and 2.0 (bottom) vs ρ close to the respective critical temperature, i.e., $T=0.165$ and 0.092.

The latter behavior is analogous to the 3D system. For sufficiently large ν the formation of rodlike aggregates already occurs at low concentrations. The stiffness measured in terms of the persistence length increases with increasing ν (cf. Ref. [11], where the liquid crystalline phase behavior of these stiff rodlike aggregates was studied in detail for the 3D system). In 2D as in 3D, the excluded volume interaction induces orientation ordering, which can be explained by an extension of Onsager's theory of the isotropic-to-nematic transition for rodlike colloidal particles [18].

Hexagonal positional order can be measured via

$$q_{\text{hex}}^{\text{pos}} = \frac{2}{N(N-1)}\left\langle \sum_{i<j} \cos(\vec{g}_{\text{hex}} \cdot \vec{r}_{ij})\right\rangle, \tag{8}$$

where $\vec{r}_{ij}$ is the vector connecting two sites i and j, and $\vec{g}_{\text{hex}}$ is a basis vector of the reciprocal hexagonal lattice in two

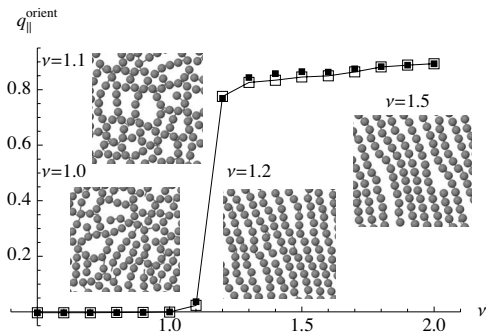

FIG. 4. $q_\parallel^{\text{orient}}$ plotted vs ν at $T=0.092$ and $\rho=0.537$. The insets show simulation snapshots obtained for the different ν values.

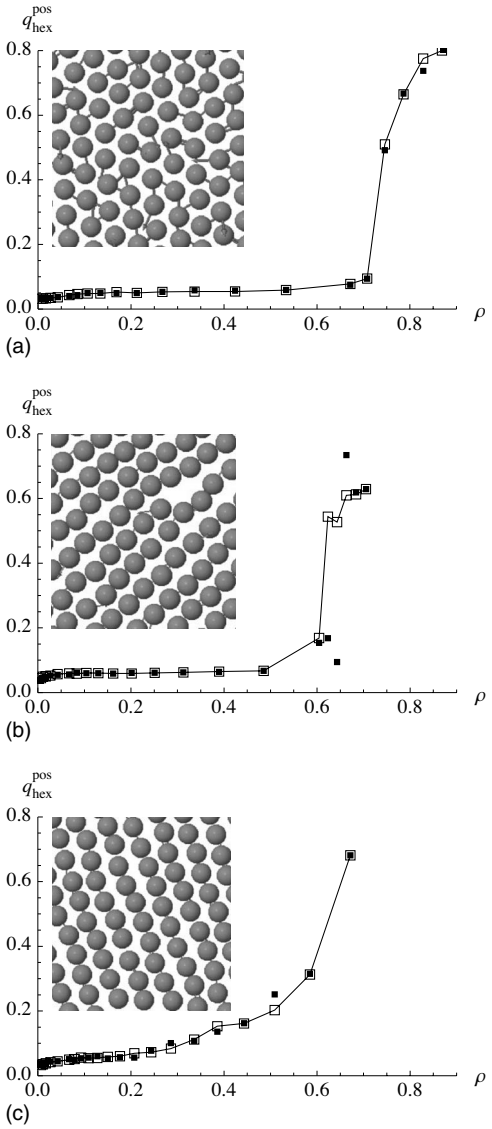

FIG. 5. Position hexagonal order parameter, $q_{\mathrm{hex}}^{\mathrm{pos}}$, vs density, ρ. Top: $\nu=0.5$, $T=0.165$ (inset density $\rho=0.873$); middle: $\nu=1.0$, $T=0.092$ (inset density $\rho=0.696$); bottom: $\nu=2.0$, $T=0.092$ (inset density $\rho=0.655$).

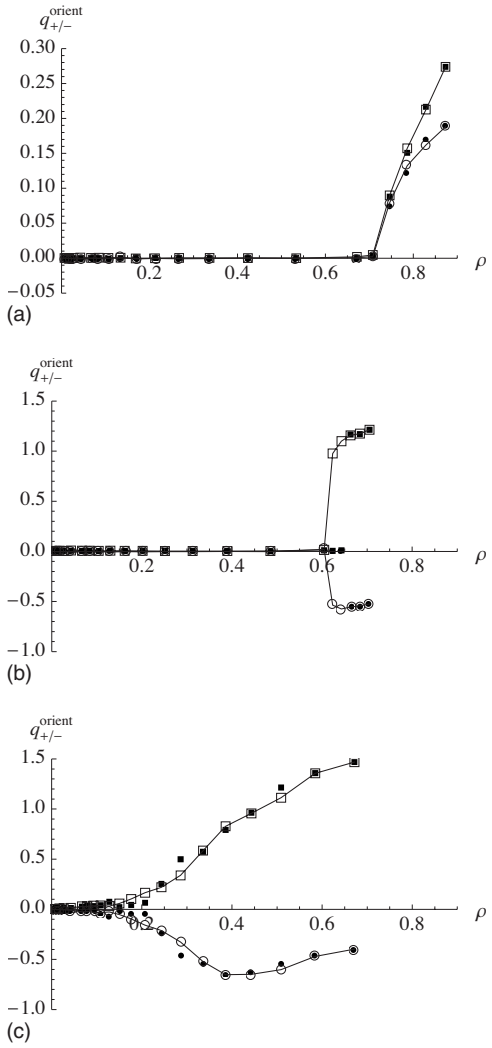

FIG. 6. Order parameters, $q_{\pm}$ (+: squares, −: circles), vs density, ρ. Top: $\nu=0.5$, $T=0.165$; middle: $\nu=1.0$, $T=0.092$; bottom: $\nu=2.0$, $T=0.092$. The meaning of filled as compared to hollow symbols is the same as in the previous figures.

dimensions. Figure 5 shows $q_{\mathrm{hex}}^{\mathrm{pos}}$ versus scaled density, ρ, for different ν. For small ν (here $\nu=0.5$) we find a first-order transition (detected via a clearly discernible jump between pressure branches along the isotherms) into a hexagonal crystalline structure, which is governed by the isotropic repulsive interaction. The anisotropic attraction matters little, as can be seen from the isotropic distribution of the $\vec{n}_i$ vectors on the hexagonal lattice induced by the repulsive interactions. Notice also that the density value at which $q_{\mathrm{hex}}^{\mathrm{pos}}$ strongly increases, $\rho \approx 0.7$, is in accord with the location of the freezing transition in the 2D LJ system studied previously [19]. Toxvaerd finds a narrow coexistence region centered at a number density of 0.8 (0.825) for temperatures close to 0.5 (1.0).

At large ν (here $\nu=2.0$) the particles associate into stiff linear aggregates forming clusters of aligned and interdigitated chains. This causes $q_{\mathrm{hex}}^{\mathrm{pos}}$ to rise more gradually. In addition, there is competition between the isotropic repulsion between the individual particles and the interaction between neighboring chains.

Finally, we introduce

$$q_{\mathrm{hex}}^{\mathrm{orient}} = \frac{2}{N(N-1)} \left\langle \sum_{i<j} [2\cos^2(3\Delta\phi_{ij}) - 1] \right\rangle, \tag{9}$$

where $\Delta\phi_{ij}$ has the same meaning as in Eq. (7), to detect hexagonal ordering of the $\vec{n}_i$. In order to distinguish hexagonal orientation from nematic ordering, it is more useful, however, to study the quantities

$$q_{\pm}^{\mathrm{orient}} = q_{\mathrm{hex}}^{\mathrm{orient}} \pm q_{\parallel}^{\mathrm{orient}}. \tag{10}$$

Notice that $q_{\pm}^{\mathrm{orient}}=0$ for isotropic orientation and $q_{\pm}^{\mathrm{orient}}=1$ in the case of hexagonal orientation ordering. On the other hand, $q_{-}^{\mathrm{orient}}=0$ and $q_{+}^{\mathrm{orient}}=2$ in the nematic case. Figure 6, in analogy to the previous figure, shows $q_{\pm}^{\mathrm{orient}}$ versus ρ. In the top panel, $\nu=0.5$ and $T=0.165$, there is little difference be-

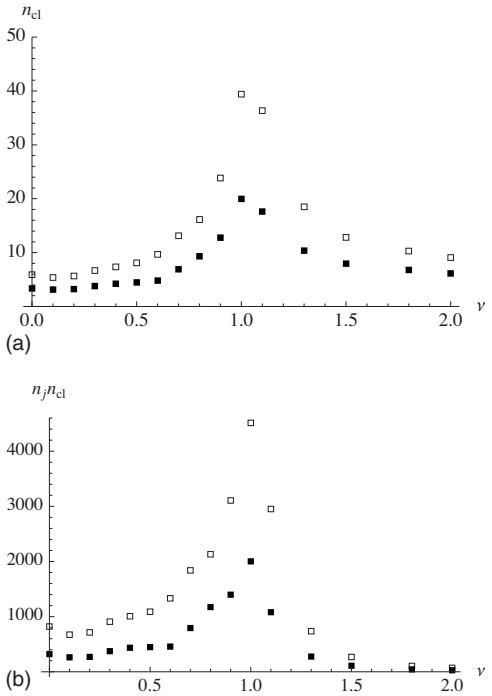

FIG. 7. Top: number average cluster size, n_{cl}, plotted vs ν. The density is constant (open squares: $\rho=0.202$; solid squares: $\rho=0.134$). For $\nu \leqslant 1$, the temperature is the GL critical temperature at the corresponding ν; for $\nu>1$, where no GL critical point is observed, the temperature is 0.092. Bottom: corresponding number of network junctions, n_j, times n_{cl} vs ν.

tween q_+^{orient} and q_-^{orient}, indicating hexagonal orientation order above $\rho \approx 0.67$. Note that $q_{\parallel}^{\text{orient}}$ is zero for isotropic distribution below $\rho \approx 0.67$ as well as for the hexagonally isotropic orientation (cf. the inset in the top panel of Fig. 5) causing $q_{\text{hex}}^{\text{orient}}$ to increase above $\rho \approx 0.67$. In the two lower panels of Fig. 6, i.e., $\nu=1.0$, 2.0 and $T=0.092$, q_+^{orient} is significantly different from q_-^{orient} above a certain concentration. Notice that q_-^{orient} becomes negative instead being close to zero. This is because $q_{\text{pos}}^{\text{orient}}$ is more sensitive to deviation from perfect nematic order, in which case it is 1, in comparison to $q_{\parallel}^{\text{orient}}$. Overall, however, the splitting indicates nematic orientational order. Comparison of this result to the alignment transition of 2D hard spherocylinders [20] is not straightforward, because the aggregates in this work are polydisperse, soft-repulsive, and, even if ν is large, persistent flexible, but nevertheless worth addressing. The relevant hard-particle result to compare with is shown in Fig. 6 of Ref. [20]. The authors find a 2D isotropic-to-nematic transition in the volume fraction range between 0.6 and 0.4 for cylinder aspect ratios between 8 and 16. Their spherocylinder volume fraction is roughly comparable to our monomer number density. From Fig. 7 (top) we see that the average aggregate size for $\nu=2$ is around 10 for densities close to 0.2. For an aspect ratio of 10, Bates and Frenkel predict the isotropic-to-nematic transition at a volume fraction close to 0.5. Because our aggregates grow with increasing density (cf. Fig. 7), we can expect the isotropic-to-nematic transition to lie in the density range between 0.2 and 0.5. This is accord with the lowest panel in our Fig. 6.

We conclude thus far that the phase behavior depends strongly on ν. For ν roughly smaller than 0.5, the system behaves like the simple LJ fluid. For larger ν up to values close to 1, we observe association of monomers into reversible networks and a crystalline phase of rodlike aggregates at high densities. For still larger ν, the monomers assemble into rather stiff linear aggregates growing in length and undergoing orientational ordering driven by their excluded volume interaction as previously observed in 3D.

The range of ν values over which we do observe network formation is quantified in Fig. 7. The top panel of this figure shows the number average cluster size, n_{cl}, plotted versus ν at constant density. Two particles are considered neighbors in a cluster if their distance is less than $0.17r_{cut}$. Variation of this criterion alters n_{cl} quantitatively but not qualitatively. The peak around $\nu=1$ thus represents the formation of large clusters. At small ν the collisions of particles prevents n_{cl} from vanishing, whereas at large ν the observed clusters are linear rods. The latter are suppressed if n_{cl} is weighted by the number of junctions as shown in the bottom panel.

IV. RELATION TO THE TLUSTY-SAFRAN TRANSITION

Some years ago, Tlusty and Safran introduced the idea of defect-induced phase separation in fluids of reversibly assembling monomers capable of forming flexible linear strands including branch points [14]. They applied this idea to the special case of dipolar fluids. According to their model, threefold end-to-end linking of chains of dipolar particles should lead to the formation of reversible networks. These networks, according to TS, may be characterized in terms of the density of the junctions and the density of free ends. Both junctions and free ends are considered defects with respective energies ϵ_3 and ϵ_1. TS develop a model in which the two types of defects compete and lead to phase coexistence between an end-rich-junction-poor phase and an end-poor-junction-rich phase. According to them, a crucial test of their model in experiment or simulation may be the observation of dipolar networks in the vicinity of the critical point in both coexisting phases.

The insets on the left in Fig. 4 show simulation snapshots obtained for $\nu=1.0$ and 1.1 at $T=0.092$ and $\rho=0.537$. The particles indeed form networks with clearly discernible threefold junctions. Moreover, Fig. 8 shows analogous snapshots at $T=0.094$ for the two coexisting densities as obtained according to the Maxwell construction method. We note that Fig. 8 is in accord with the picture underlying the TS transition. A more detailed comparison of these simulation results to the predictions of the TS model therefore appears interesting.

TS find the following critical quantities in terms of the defect energies:

$$T_c^{\text{TS}} = \frac{\epsilon_1 - 3\epsilon_3}{\ln[27/4]}, \tag{11}$$

$$\ln \phi_c^{\text{TS}} = -\frac{\epsilon_1 \ln[9/2] - \epsilon_3 \ln[2]}{\epsilon_1 - 3\epsilon_3}, \tag{12}$$

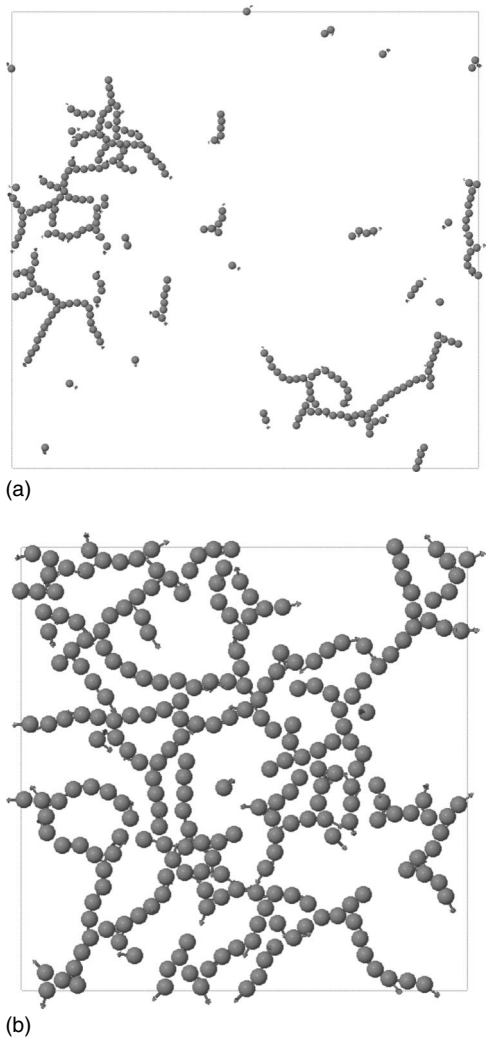

FIG. 8. Simulation snapshots obtained for $\nu=1.0$ at $T=0.094$ on the coexistence curve (top: $\rho=0.048$; bottom: $\rho=0.284$).

$$\ln P_c^{\mathrm{TS}} = -\frac{\epsilon_1 \ln[81/2] - \epsilon_3 \ln[32]}{\epsilon_1 - 3\epsilon_3}. \tag{13}$$

Note that ϕ_c^{TS} is the critical volume fraction related to the critical number density by $\rho_c^{\mathrm{TS}}=b^{-1}\phi_c^{\mathrm{TS}}$, where b is the particle volume. In order to compare this to our results, we need to estimate ϵ_3 and ϵ_1 based on our model potential. We consider the interaction between two particles at fixed orientation, i.e., $u=4(r^{-12}-\kappa r^{-6})$. The optimized potential energy follows via $du/dr|_{r=r_{\min}}=0$, which yields $u_{\min}=-\kappa^2$. For parallel or antiparallel orientation we have $u_{\min}=-\mu^2$. The potential energy of a reversible chain consisting of n bonds may thus be approximated by $-n\mu^2$. Cutting the chain at a particular bond creates two free ends, i.e., $2\epsilon_1 \approx -(n-1)\mu^2 - (-n\mu^2)=\mu^2$. Similarly we may estimate ϵ_3 by cutting two bonds, thus creating three pieces of chain, and subsequent fusion of three of the ends, i.e., $\epsilon_3 \approx -(n-2)\mu^2 - (-n\mu^2) - 3\mu^2(3/4)^{2\nu}=[2-3(3/4)^{2\nu}]\mu^2$. The last term, the fusion energy, assumes three particles at the corners of an equilateral triangle whose $\vec{n}$-vectors are in the plane of the triangle and forming 30 (or 150) degree angles with the sides of the triangle.

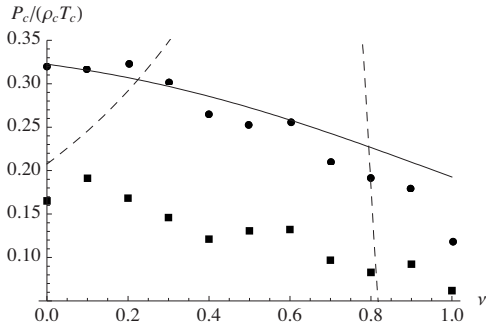

FIG. 9. $P_c/(\rho_c T_c)$ vs ν (circles: 3D; squares: 2D). The dashed line is the result obtained according to the TS theory. The solid line is the theory developed in Ref. [13].

According to this estimate, $T_c^{\mathrm{TS}} \propto \mu^2$ in agreement with Eq. (3). The particle volume b for our model may be estimated via $b=\pi(r_o/2)^2=(\pi/4)(\mu\lambda)^{-1/3}$, where r_o is the solution of $r_o^{-12}-\mu\lambda r_o^{-6}=0$. Notice that λ is computed above. Again we obtain $\rho_c^{\mathrm{TS}} \propto \mu^{1/3}$ as required by Eq. (4). The dashed lines in Figs. 2 and 9 show the final result of this mapping of the TS critical parameters onto our model. When ν is roughly smaller than 0.5, we do not find network formation in the simulation and thus we do not expect the TS theory to apply. However, for larger ν up to $\nu \approx 1.1$, where the behavior changes completely, we do find network formation. The fact that simple scaling using rotationally averaged attraction leads to far better agreement with the simulation results for the critical parameters in the entire range of ν values strongly suggests that the competition between free ends and junctions is not the driving force behind phase separation in the present system.

Figure 9 shows the critical compressibility factor, $P_c/(\rho_c T_c)$, as obtained from the simulated coexistence curves in 2D and 3D. A comparison of this quantity for the 2D LJ system ($\nu=0$) can be made based on Ref. [21], where the authors compile the critical quantities for this system as obtained previously by a number of groups. The range is roughly $0.19 < P_c/(\rho_c T_c) < 0.25$. Our own data agree with this if they are represented by a straight line fit. A straight line fit also shows a decrease of $P_c/(\rho_c T_c)$ with increasing ν. Again the dashed line is the result obtained via the TS method. This curve has a maximum around $\nu \approx 0.5$ (cut off in the figure) above which it drops steeply.

One may argue at this point that the above computation of the TS defect energies is rather rough. This together with the somewhat fuzzy range of ν values for which network formation is observed may account for some of the overall discrepancy between the TS predictions and the simulation results. However, there is still another reason suggesting a driving force behind phase separation other than the junction-free ends competition underlying the TS theory.

Notice that the simulation data in Figs. 2 and 9 show a rather smooth dependence on ν from $\nu=0$, where the systems undergoes normal GL phase separation, to $\nu=1$, where the nature of the transition may be different. Because the TS mechanism for phase separation is very different from GL

phase separation in simple liquids, we would expect a discernible discontinuity in the T_c versus ν and ρ_c versus ν curves. This is not the case. We add that in a recent computer study of monolayers of dipolar particles, Duncan and Camp also do not find evidence for a TS transition under equilibrium conditions [9].

V. RELATION TO GL PHASE BEHAVIOR OF LINEAR CHAINS

Recently we studied the 3D version of this model [13]. Figures 1 (top panel) and 2 (top and middle panel) in Ref. [13] show results corresponding to the 2D results in Figs. 1 and 2. In 3D and in 2D the dependence of the GL critical point on ν is qualitatively the same. In particular, the deviations of the simulation results from the scaling approximations based on rotationally averaged attraction are qualitatively the same in both dimensions. Notice that T_c(3D) is roughly twice T_c(2D) due to the roughly doubled number of nearest neighbors (doubling of attractive interaction) in 3D as compared to 2D. The critical densities are roughly the same in 2D and in 3D, because the particle size is independent of dimension. Here we argue along the lines of the van der Waals theory, which of course is a crude description, as the dependence of the critical compressibility factor on dimension in Fig. 9 illustrates.

In 3D, we were able to explain the deviation of T_c and ρ_c from the scaling approximation [here Eqs. (5)] in terms of the theory of lattice polymer thermodynamics developed by Flory and co-workers many years ago [22], but now extended by terms in the free energy accounting for reversible assembly of monomers into polydisperse chains [13,23]. For instance, according to Flory, $P_c/(\rho_c T_c) \sim n^{-1}$ in the case of linear polymers of length n (for large n). In the case of reversible chains, n is replaced by the average length, which in turn is $n=1/2+1/2\sqrt{1+4\phi_{\text{solute}}\exp[-\Phi_o]}$. Notice that here n is the number average size, ϕ_{solute} is the monomer volume fraction, and Φ_o is the free enthalpy contributed (in units of T) per reversible monomer-monomer contact along the chain. The latter may be tied to ν as shown in Ref. [13]. In general, n increases as ν decreases (cf. Fig. 5 in Ref. [13]). Using the theory explained in Ref. [13], we compute the solid line in Fig. 9, i.e., the 3D compressibility factor is reproduced quite reasonably [24]. Thus we conclude that the decrease of the critical compressibility factor in Fig. 9 is consistent with the formation of reversible chains near criticality. Unfortunately, the Flory lattice theory, the basis of our theoretical model of reversibly assembling polymers, is not sensitive to dimension—a general feature of mean-field theories. In addition, it does not include non-chain-like aggregates. Nevertheless, combining the similarity of the 2D to the 3D results with the theory linking the observed dependence of GL critical parameters to the formation of reversible chains in 3D, we conclude that the ν-dependent reversible aggregation is responsible for the analogous behavior in 2D rather than a novel mechanism due to competition between cross-links and free ends in a network.

VI. CONCLUSION

We have studied the phase behavior of a model fluid with adjustable anisotropic inter-particle attraction in two dimensions extending a previous computer simulation study of the same model in 3D. The anisotropy of attraction may be controlled by a parameter ν. If ν is increased from zero, where the particles interact via a truncated LJ potential, the attraction is increasingly constrained to a narrowing cone of orientations. This causes the reversible formation of chains and, in addition in 2D, networks. For small ν the system behaves LJ-like, whereas for large ν the chainlike aggregates interact mainly via excluded volume leading to nematic alignment and crystalline packing at high densities. In the intermediate ν range, we find the formation of network structures in 2D. Similar network formation has been observed earlier in the 2D dipolar hard-sphere system [10,25,26]. In this system, the occurrence of ringlike clusters and subsequent contact formation between clusters upon increasing density appears to be the dominant type of network formation rather than the formation of Y-shaped junctions observed here. In Ref. [10], the authors in particular discuss the possibility of a phase transition from disconnected clusters to networks of spanning clusters. In the present work, we have attempted to describe the observed shift of the critical parameters with ν on the basis of a defect theory due to Tlusty and Safran. It appears, however, that the observed ν dependence of the critical parameters is due to the formation of reversible aggregates, particularly chains or chain segments, rather than to the competition between cross-links and free ends in a network.

[1] C. Holm and J.-J. Weis, Curr. Opin. Colloid Interface Sci. **10**, 133 (2005).

[2] J.-J. Weis and D. Levesque, in *Advanced Computer Simulation Approaches for Soft Matter Sciences II*, edited by C. Holm and K. Kremer, Advances in Polymer Science Vol. 185 (Springer, New York, 2005).

[3] P. I. C. Teixeira, J. M. Tavares, and M. M. Telo da Gama, J. Phys.: Condens. Matter **12**, R411 (2000).

[4] G. Bossis, B. Quentrec, and C. Brot, Mol. Phys. **39**, 1233 (1980).

[5] A. Bradbury, S. Menear, and R. W. Chantrell, J. Magn. Magn. Mater. **54-57**, 745 (1986).

[6] G. T. Gao, X. C. Zeng, and W. Wang, J. Chem. Phys. **106**, 3311 (1997).

[7] S. H. L. Klapp and M. Schoen, J. Chem. Phys. **117**, 8050 (2002).

[8] J.-J. Weis, J. Phys.: Condens. Matter **15**, S1471 (2003).

[9] P. D. Duncan and P. J. Camp, Phys. Rev. Lett. **97**, 107202 (2006).

[10] J. M. Tavares, J.-J. Weis, and M. M. Telo da Gama, Phys. Rev. E **73**, 041507 (2006).

[11] B. Fodi and R. Hentschke, J. Chem. Phys. **112**, 6917 (2000).

[12] N. Boden, in *Micelles, Membranes, Microemulsions, and Monolayers*, edited by W. M. Gelbart, A. Ben-Shaul, and D. Roux (Springer-Verlag, New York, 1994).
[13] W.-Z. Ouyang and R. Hentschke, J. Chem. Phys. **127**, 164501 (2007).
[14] T. Tlusty and S. A. Safran, Science **290**, 1328 (2000).
[15] Y.-S. Wei and R. J. Sadus, AIChE J. **46**, 169 (2000).
[16] M. Ley-Koo and M. S. Green, Phys. Rev. A **23**, 2650 (1981).
[17] M. Rovere, D. W. Heermann, and L. Binder, J. Phys.: Condens. Matter **2**, 7009 (1990).
[18] L. Onsager, Ann. N.Y. Acad. Sci. **51**, 627 (1949).
[19] S. Toxvaerd, J. Chem. Phys. **69**, 4750 (1978).
[20] M. A. Bates and D. Frenkel, J. Chem. Phys. **112**, 10034 (2000).
[21] M. R. Reddy and S. F. O'Shea, Can. J. Phys. **64**, 677 (1986).
[22] P. J. Flory, *Principles of Polymer Chemistry* (Cornell University Press, Ithaca, NY, 1953).
[23] R. Hentschke, J. Bartke, and F. Pesth, Phys. Rev. E **75**, 011506 (2007).
[24] For $n=1$, the Flory equation of state yields $P_c/(\rho_c T_c)=2\ln 2-1\approx 0.386$. This value is larger than the value in the figure for $\nu=0$. This is because the theory does not quite reach the limit $n\to 1$. The reason behind this is explained in detail in the paragraph below Eq. (10) in Ref. [23].
[25] J. J. Weis, Mol. Phys. **100**, 579 (2002).
[26] J. J. Weis, Mol. Phys. **93**, 361 (1998).